手段です．

「品質に影響を及ぼす」といった言葉がしばしば使われますが，この「品質に影響を及ぼす」とは，有効性・安全性に影響を及ぼすか否かを基準に考えるべきことであると，視点を変えれば確保すべき品質の範囲は，有効性/安全性が認められた製品の品質特性に基づいて定められるものである，といったコンセプトになります．

効果的に品質確保，つまり安全性・有効性の継続的保証を図るための手段としては，製品レベルや製造工程レベルでの相互補完的な恒常性維持・管理方策がポイントとなります．

具体的には，有効性/安全性確保に必要な製造工程部分，あるいは工程管理法，規格及び試験方法等を合理的，効率的にバランスよく設定し，GMP で管理し，変更がある場合は必要な検証を実施する，ということになります（Fig. 2）．

こうしたコンセプトは，ICH Q5E や Q6B，その他のガイドラインにも一貫して流れているものでありますし，過日の承認申請書記載要領説明会でこの図とともに同様の説明がなされたもので，ここでも再確認しておくべき最も基本的なことであると思います．

4.2　医薬品品質確保方策全体の中で製造方法が果たす役割と位置づけの再確認

次に，医薬品品質確保方策全体の中で製造方法が果たす役割と位置づけの再確認をしておきたいと思います．

Fig. 3 はバイオ医薬品の品質確保方策全体を構成する要素を示したものです．

先にも述べましたように，効果的に品質確保を図るためには，製造レベルあるいは製品レベルの相互補完的な恒常性維持と管理方策がポイントとなります．このうちどの要素に重きを置く，あるいはどのような要素の組み合わせで品質確保を図るかは，一義的に製造業者が選択して，その妥当性をいかに示すかにかかっています．しかしながら，品質確保がある製造工程に依存する場合は，自ずとそれを選択することとなります．

例えば，①ウイルス等の微生物混入否定，特殊な製剤機能の確保など製品レベルでは必要十分な品質評価・保証が困難な場合，②工程由来不純物に関す

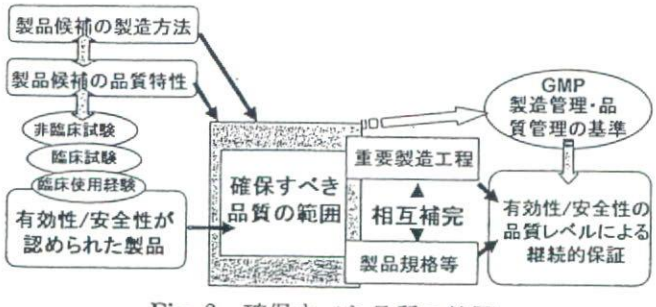

Fig. 2　確保すべき品質の範囲

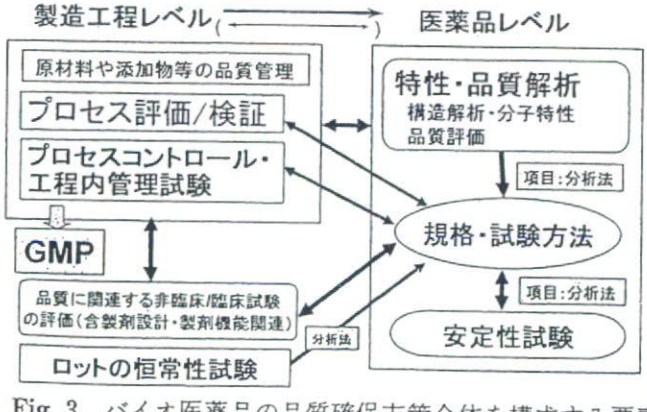

Fig. 3　バイオ医薬品の品質確保方策全体を構成する要素

る限度試験，製品レベルで試験困難な事項など製造工程レベルで評価・保証する方がより合理的な場合，③製品の安定性保証が製造工程の中にデザインされている（製品レベルでの日常の品質特性評価試験では直ちに品質の経時的変化が検出できない）場合などがそれに当たります．

一般のケースでの製造工程への依存度は，製品での品質保証・管理と製造工程パラメータ等での品質保証・管理それぞれのウエイトの置き方，組み合わせ方を製造者が選択し，その妥当性をいかに立証するかによって定められます．

特に原薬の場合，極端な例では薬局方の承認不要品目のように規格及び試験方法だけで目的を達することもできますし，正反対の極端な例では製造工程のパラメータだけで目的を達することも可能かも知れません．

4.3　同一線上にない各極の承認制度や方針の認識及びCTDM3，QOS，承認書と製造方法の取扱いの整理

次に別の切り口として考えておかなければならないこと，そしてきわめてcriticalなこととして同一線上にはない各極の承認制度や方針を認識すること，更にCTDの第3部，QOS，承認書と製造方法の取扱いの整理が挙げられます．

周知のことですが，CTDの構成をFig. 4に示します．第3部が品質に関する文書，第2部の2.3が品質に関する概括資料，いわゆるQOSと呼ばれるものです．これらは，承認申請における添付資料作成のための必要な項目とその配列順序を示すものですが，特定の必要なデータの種類や程度について規定したものではありませんし，承認申請書に言及するものでもありません．その理由は，各極の承認審査制度あるいは承認事項や内容が実態と異なることを踏まえたからです．当時，欧米では第3部を主体に審査し，QOSはほとんど活用しないとのことでした．もし第3部の内容を要求事項としてICHで調和しようとすると，我が国は審査のあり方を変える必要がありますし，リソースもとても間に合わないということで，我が国の実態に抵触しないように主張し続けた結果，その取扱いは各国の方針に委ねるとした現在の方式となりました．しかし，それに対して，今またある種の揺り戻しが来つつあるような感じがしております．

我が国では，第3部はあくまで審査に必要な添付資料であります．一方，QOSも添付資料ですが，現実にはこれを最大限活用して効率的な審査をしています．そして，法的な拘束力のある承認事項は承認申請書に記載された事項，内容です．承認申請書には用法及び用量，効能又は効果等がもちろん記載されていますが，承認時のこうした有効性・安全性の継続的保証は，専ら品質レベルでの継続的保証によるということですので，品質確保に関する規格の

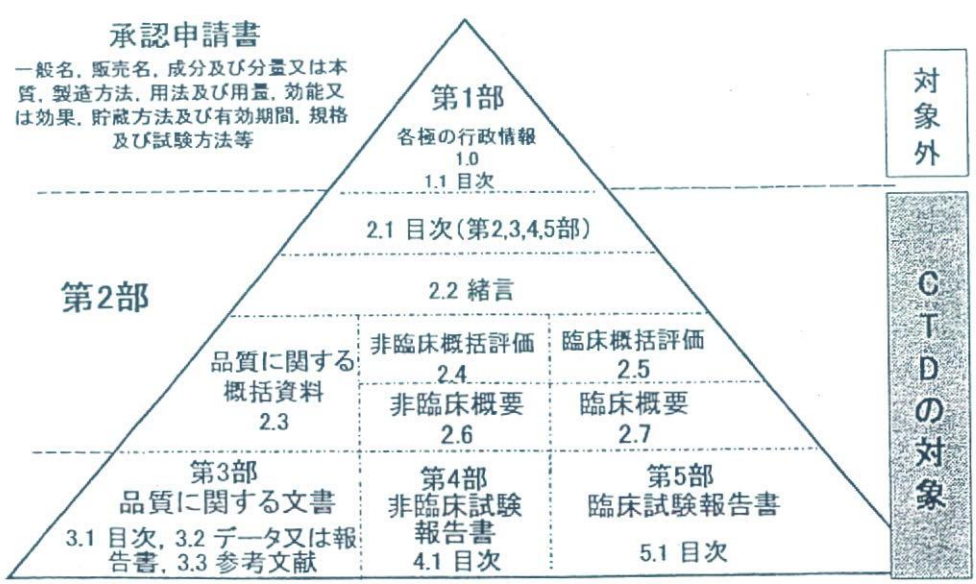

Fig. 4　承認申請書及び添付すべき資料の構成

設定や製造方法の内容に承認書の大半が割かれることになります．

しかし，製造方法を第3部のように，ただ詳細に記載すれば良いというものではありません．製品の品質規格との相互補完性を合理的に考え，品質確保に必要な事項に着目して記載するべきものであるということであります．

製造方法については，我が国では第3部のエッセンスをQOSに，QOSのエッセンスが承認申請書に記載され承認事項となります．逆にいえば第3部やQOSで記載された製造方法のうち，承認申請書の製造方法欄に記載されなかった事項は承認事項にはなりません．例えば製造過程での各種の社内基準や処置基準値などは承認事項ではありませんので，承認事項の一部変更の申請の対象とはなりません．

このことはCTD-Qを説明する際に繰り返し説明してきたところであります（Table 7～10）．この見解の微調整はともかくとして，状況は基本的に変わるものではないと思っています．

Table 7　3.2.S.2.2　製造方法及びプロセスコントロール

本項の製造方法の記載内容と承認申請書の記載内容の詳細さの違いに関して，

本項には一連の製造方法を記載する．承認申請書は，従来と同様，製品の品質を確保する上で重要な工程，プロセス・コントロール等を適宜記載する．

従って，本項の内容の中で，例えば，出発物質及び中間体の仕込量，収率，試薬の仕込量，原材料・溶媒・触媒・試薬の量，詳細な操作条件などについては，必ずしも承認申請書に記載する必要はない（規格の設定など全体からみて品質確保策が十分講じられている場合）．

Table 8　3.2.S.2.4　重要工程及び重要中間体の管理

- 重要工程，重要中間体が管理されていることを保証する管理方法・基準のうち，特に必要なものについては規格/判定基準及び試験方法を設定し，承認申請書に記載する．
- 承認申請書に記載した場合，最終製品の規格及び試験方法に代わりうる．
- 処置基準値等は社内管理の対象であり承認申請書に記載する必要はない．

Table 9　重要工程とは

- 無菌工程・滅菌工程
- 再加工工程
- 適切な管理を保証するため申請者が定めた工程
- 試験方法及び規格を設定した工程
- ウイルス不活化・除去工程

Table 10　3.2.S.2.5　プロセス・バリデーション／プロセス評価

- 無菌工程及び滅菌工程のプロセス・バリデーションやプロセス評価について記述する．
- 生物薬品：製造工程（再加工を行う工程を含む）が目的に適しているかどうかを証明し，重要なプロセスコントロール法（操作管理項目及び工程内管理試験）を選択し，重要な製造工程（細胞培養，ハーベスト，精製，修飾等）における判定基準の妥当性を実証するためのバリデーション及び評価試験に関する十分な資料を示す．
- 試験計画並びに試験の結果，考察及び結論を記述する．試験方法とそのバリデーションについては，相互参照できるようにするか，又は重要なプロセスコントロール法の選択及び規格／判定基準の妥当性を示す資料の一部として記述する．
- ウイルス汚染を除去又は不活化する製造工程について，ウイルスクリアランス評価試験に関する資料を3.2.A.2にて示すこと．

4.4　開発時，承認審査時，市販後の各段階における製造方法問題のとらえ方（Table 11）

次に，もしICHガイドラインを作成するとした場合，開発時，承認審査時，市販後の各段階における製造方法問題を我々ならどう捉えるかについて，仮に整理しておきたいと思います．

開発段階では，製品開発及び製品の品質確保を最も合理的・効果的に行うために開発段階でどのような考え方，アプローチで製造方法をデザインしていけばよいかが課題となりますが，これは主に企業側の課題であり，承認のための評価に直接関係する重要事項や背景データ以外はガイドラインの対象外としてはどうかと思っています．

承認審査段階のものが，まさにガイドラインの対象となるべきものであります．有効性・安全性との関係において承認条件として確保すべき品質の範囲について，①製品の品質特性面，②製造方法面，③製品面と製法面の相互補完関係からいかに合理的，

Table 11　開発時，承認審査時，市販後の各段階における製造方法問題のとらえ方

- 開発段階：製品開発及び製品の品質確保を最も合理的・効果的に行うために開発段階でどのような考え方，アプローチで製造方法をデザインしていけばよいか(主に企業側の課題)：承認のための評価に直接関係する重要事項や背景データ以外はGL対象外
- 承認審査段階：有効性・安全性との関係において承認条件として確保すべき品質の範囲を①製品の品質特性面，②製造方法面，③製品面と製法面の相互補完関係から，いかに合理的，効果的に定めていくか（適切な資料提供と評価に関する企業側と審査側の共通認識と理解）：GLの対象
- 市販後：承認条件として確保すべきとされた品質（特性）の製品を恒常的に生産するための製造現場における製造管理及び品質管理の基準（主に企業側の課題）GL対象外
- 製法変更：コンパラビリティ問題又はGMPの変更管理問題

効果的に定めていくのか，それに関わる適切な資料提供と評価に関する企業側と審査側の共通認識と理解が非常に重要である，との視点でガイドラインを作成する必要があると思います．

市販後は，承認条件として確保すべきとされた品質（特性）の製品を恒常的に生産するための製造現場における製造管理及び品質管理の基準が課題となりますが，主にGMP問題であり，企業側の課題でもありますので，今回のガイドラインの対象外と考えます．

製法変更については，既にコンパラビリティ問題又はGMPの変更管理問題として，Q5EあるいはQ7の中で検討されているとして整理したいと思います．

ICHで原薬の製造方法問題を取り上げるとすれば，承認審査段階に絞り，かつ各極が承認事項として共通に考えられる品質とその恒常性確保に必要な要件とは何か，その中での製造方法の位置づけとその背景をなすコンセプトなどにおいて合意が得られるという前提条件が必要であると考えています．

そしてそれに関連して，整理しておくべきことをFig. 5に示しています．

まず，承認事項としての品質と恒常性確保要件とは，あくまで評価された製品の安全性・有効性を品質レベルで継続的に保証することを目的とした品質特性と製造方法のエッセンスで構成されるべきという視点，あるいはコンセプトを持つことが極めて重要であると思っています．

この要件の中には，製品の品質特性のエッセンスの反映という面では規格及び試験方法があります．製造方法面では，ケースにもよりますが，含まれるべき要素としてプロセス評価/検証，重要工程の一定性，プロセス・コントロール，工程内管理試験，更には原材料や添加剤の品質・安全性の確保問題があります．

また，この品質確保のコア要素やその組み合わせを，どのような考え方で承認要件として定めるべきなのか，必要な背景情報としての製造方法に関する

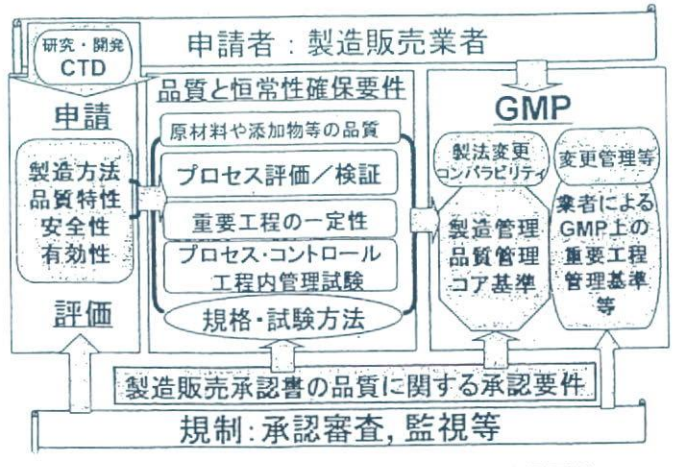

Fig. 5　承認事項としての品質とその確保要件

資料をいかに申請時に過不足なく提出すべきなのかに関するガイドライン作りが果たしてできるかどうか，我が国の承認制度に抵触しないかどうか，などについて注目して対応していく必要があります．

繰り返しになりますが，品質確保のコア基準とは，あくまで安全性，有効性を保証するための品質確保との視点から見て最小限必要な要素のエッセンスであり，これらをいかにきちんと承認申請書に盛り込み，その妥当性を説明するかが申請者の腕の見せ所であり，いかに適正に評価して合理的な承認要件とするのかがレビューアの腕の見せ所であります．

この承認要件は当然のことながらGMPにも直結し，必然的にGMP上で絶対守るべき製造管理，品質管理のコア基準となります．これは必ずクリアする必要があります．そうしなければ承認事項の逸脱になります．業者としてはこのコア基準，すなわち承認事項からの逸脱がないように，更に独自にGMP上の重要工程や管理基準等を設け，いかに合理的に変更管理を行っていくかを考えなければなりません．

なお最近の記載要領を見ると「重要工程」という言葉が記載されています．その定義は，「規格に適合することを保証するための工程」とされていますので，主に業者により重要であるとして独自に設定されたGMP上の工程を指すと考えられます．その点についても留意しながら議論を進めていく必要があると思っています．

5．品質確保と製造方法問題の視点

ガイドラインを作るとした場合の品質確保と製造方法問題の視点を改めてまとめておきたいと思います．

まず，最上位概念は「有効性・安全性確保のための品質確保」であります．「品質の品質による品質のための」との思考に陥らないようにしなければいけません．

2点目は，医薬品品質確保方策全体の中で製造方法が果たす役割と位置づけに関する考え方の確認です．

3点目は，開発時，承認時，市販後（GMPを含む）の各段階のうち，主に承認審査段階における製造方法問題に焦点を当てるということです．

4点目は，CTD第3部，QOS，承認書のうち，承認書の中で承認要件として定める製造方法関連事項に焦点を当てることです．

CTDの第3部をベースとして審査を行い，承認事項としてきた欧米では，産官とも合理化，効率化を目指した域内でのパラダイムシフトとともに，その政策のICHレベルでの浸透を試みようとしているように思われます．

一方，我々は，品質，特に製法の取扱い問題は，各極の承認事項や承認制度の根幹にふれる側面を持つことを明確に認識，整理しておく必要があります．我が国が欧米の動きにどこまで歩調を合わせるのか，合わせないのかについて，国益，国際益のバランスシートにかけるビジネスプランにより事前評価しておく必要があります．

CTD第3部のエッセンスをQOSに，QOSのエッセンスを承認事項としてきた我が国の承認制度や承認書は，リソースに乏しい我が国で工夫された合理性の極致といえます．QOSの合理性，効率性が最近見直されていることは，その現れであると思います．我が国のそうした優れた方策に更に磨きをかけることができるのであれば，ICHを行ってもよいとの視点で問題をとらえるべきではないかと思っています．

6．まとめ

共通の目標，その背景となる基本概念，目標達成に必要な科学的原則や要素，普遍的な方策・手段に関して国際調和をすることは必要不可欠であります．

しかしながら一方で，目標達成に向かうために各極，各パーティ，各者がとる方策，手段はそれぞれの実情，合理性，効率性に合ったフレキシブルなものであるべきと思います．制度やシステムの変更に及ぶような合意への要請は国際調和活動とはいえません．

最後に最近改めて感じることですが，日本人が日本人に分かる日本語で明瞭に語り，説明でき，理解され，受け入れられるような概念や考え方，一般原則，言葉でないと我が国が行う国際調和とはいえないと思います．

もしこれから何かをやるとしても，自らの目標，概念あるいは考え方，原則，言葉を持つことが国際調和活動の前提ではないかと考えております．

Gene Therapy (2007) 14, 912–919

www.nature.com/gt

ORIGINAL ARTICLE

Downregulation of human CD46 by adenovirus serotype 35 vectors

F Sakurai[1], K Akitomo[1], K Kawabata[1], T Hayakawa[2] and H Mizuguchi[1,3]

[1]Laboratory of Gene Transfer and Regulation, National Institute of Biomedical Innovation, Osaka, Japan; [2]Pharmaceuticals and Medical Devices Agency, Tokyo, Japan and [3]Graduate School of Pharmaceutical Sciences, Osaka University, Osaka, Japan

Human CD46 (membrane cofactor protein), which serves as a receptor for a variety of pathogens, including strains of measles virus, human herpesvirus type 6 and Neisseria, *is rapidly downregulated from the cell surface following infection by these pathogens. Here, we report that replication-incompetent adenovirus (Ad) serotype 35 (Ad35) vectors, which belong to subgroup B and recognize human CD46 as a receptor, downregulate CD46 following infection. A decline in the surface expression of CD46 in human peripheral blood mononuclear cells was detectable 6 h after infection, and reached maximum (72%) 12 h after infection. Ad35 vector-induced downregulation of surface CD46 levels gradually recovered after the removal of Ad35 vectors, however, complete recovery of CD46 expression was not observed even at 96 h after removal. The surface expression of CD46 was also reduced after incubation with fiber-substituted Ad serotype 5 (Ad5) vectors bearing Ad35 fiber proteins, ultraviolet-irradiated Ad35, vectors and recombinant Ad35 fiber knob proteins; in contrast, conventional Ad5 vectors did not induce surface CD46 downregulation, suggesting that the fiber knob protein of Ad35 plays a crucial role in the downregulation of surface CD46 density. These results have important implications for gene therapy using CD46-utilizing Ad vectors and for the pathogenesis of Ads that interact with CD46.*
Gene Therapy (2007) **14,** 912–919. doi:10.1038/sj.gt.3302946; published online 22 March 2007

Keywords: *adenovirus serotype 35 vector; CD46; downregulation; fiber knob; peripheral blood mononuclear cells*

Introduction

Human CD46 is a transmembrane glycoprotein, which is ubiquitously expressed in most or all human nucleated cells. CD46 functions as a regulator of complement activation, whose normal function is to protect the host from autologous complement attack, by binding complement components C3b and C4b and facilitating their cleavage by factor I.[1,2] In addition to these functions, CD46 serves as a receptor for several pathogens, including strains of measles virus (MV),[3] human herpesvirus type 6 (HHV6),[4] group A *streptococci*[5] and *Neisseria*.[6] Among these pathogens, infection by certain strains of MV,[7,8] HHV6[4] and *Neisseria gonorrhoeae*[9] has been shown to cause CD46 downregulation from the cell surface. The detailed mechanisms of surface CD46 downregulation upon infection by these pathogens remain to be elucidated, however, the decrease in the surface density of CD46 renders the cells more susceptible to lysis by complements, as demonstrated *in vitro*,[10] and may contribute to the attenuation of these pathogens by rapid clearing of infected cells.

Recently, it has been demonstrated that CD46 also acts as a receptor for the majority of subgroup B adenoviruses (Ads), including Ad serotypes 11 (Ad11) and 35 (Ad35).[11,12] The fiber knob domain of Ad11 or Ad35 binds to short consensus repeats (SCRs) 1 and/or 2 in CD46 for infection.[13–15] Furthermore, Ad35 competes for binding to CD46 with the MV hemagglutinin (MVH) protein,[14] which is responsible for both the attachment of MV to CD46[16] and downregulation of surface CD46 expression levels.[17] These findings led us to hypothesize that CD46 is downregulated following infection by subgroup B Ads, as occurs in the case of MV. On the other hand, subgroup B Ad11 and Ad35 are considered to be an attractive framework for gene transfer vectors for the following reasons. First, Ad11 and Ad35 are known to be rarely neutralized by human sera.[18] Second, Ad11 and Ad35 exhibit a broad tropism including cells expressing no or low levels of coxsackievirus and adenovirus receptor (CAR), which is a receptor for Ads belonging to subgroups A, C, D, E and F.[19] Several groups (including the authors) have developed replication-incompetent Ad vectors composed of subgroup B Ads[20–24] or fiber-substituted Ad serotype 5 (Ad5) vectors containing subgroup B Ad fibers,[25–28] and have demonstrated that these types of Ad vectors efficiently transduce a variety of human cells, including cells refractory to conventional Ad5 vectors. If surface CD46 downregulation occurs following transduction with CD46-utilizing Ad vectors, unexpected side effects might occur such as complement-mediated cell lysis of successfully transduced cells, which leads to clearance of the transduced cells.

In the present study, we examined replication-incompetent Ad35 vector-induced downregulation of surface

Correspondence: Dr H Mizuguchi, Laboratory of Gene Transfer and Regulation, National Institute of Biomedical Innovation, 7-6-8 Asagi, Saito, Ibaragi City, Osaka 567-0085, Japan.
E-mail: mizuguch@nibio.go.jp
Received 24 September 2006; revised 7 February 2007; accepted 7 February 2007; published online 22 March 2007

CD46 expression. We found that transduction with Ad35 vectors significantly downregulated CD46 expression from the cell surface in a dose-dependent and cell type-specific manner. Ad35 vector-mediated downregulation of surface CD46 was found to occur in leukemia cells, whereas nonleukemia cells did not exhibit any decline in surface CD46 expression following Ad35 vector infection. To the best of our knowledge, this is the first report characterizing subgroup B Ad-mediated downregulation of surface CD46.

Results

Infection with Ad35 vectors causes downregulation of surface CD46 expression

To determine whether infection with Ad35 vectors results in modulation of surface CD46 expression, human peripheral blood mononuclear cells (PBMCs) were incubated with the Ad35 vector expressing green fluorescence protein (GFP) (Ad35GFP) at 10 000 vector particle (VP)/cell and subjected to flow cytometric analysis at various time points. This analysis demonstrated that the surface expression levels of CD46 in PBMCs gradually decreased during exposure to Ad35GFP (Figure 1a). The significant decrease in CD46 was detectable 6 h after infection and reached maximum 12 h after infection (72% downregulation). Furthermore, the downregulation of surface CD46 by Ad35 vectors was found to be dose dependent (Figure 1b). PBMCs infected at 1250 VP/cell showed significantly reduced levels of CD46 expression (44% downregulation), and 71% downregulation of surface CD46 expression was induced at 20 000 VP/cell. These results indicate that infection with Ad35 vectors downregulates surface CD46 expression, as happens in the cases of MV[7,8] and HHV6.[4] The viability of PBMCs was not significantly affected by Ad35 vector infection (data not shown).

Next, in order to examine whether B cells ($CD19^+$ cells) and T cells ($CD3^+$ cells) in PBMCs show a reduction in surface CD46 levels after infection with Ad35 vectors, PBMCs were simultaneously stained with anti-human CD46 and anti-human CD19 or anti-human CD3 antibodies, and were subsequently subjected to flow cytometric analysis. Surface CD46 downregulation was found in both B cells and T cells after Ad35 vector infection, but the levels of the downregulation in these cells were lower than those of whole PBMCs (Figure 1c). Surface CD46 expression in T cells was more largely reduced than that in B cells. We also investigated seven additional human cells (Molt-4, KG-1a, K562, U937, A549, HeLa and human bone marrow-derived $CD34^+$ cells) for Ad35 vector-induced downregulation of surface CD46 levels; the downregulation levels of surface CD46 were different among the cell types (Table 1). K562, U937, KG-1a and Molt-4 cells exhibited a decrease in CD46 expression following Ad35 vector infection (by 36% in K562 cells, 24% in U937 cells, 18% in KG-1a cells

Table 1 Downregulation of CD46 induced by Ad35 vectors in various types of cells

Cell type	*% CD46 downregulation*
Molt-4	55±5.7
KG-1a	18±2.6
K562	36±1.9
U937	24±8.6
A549	−10±8.0
HeLa	7.9±18
Human bone marrow-derived $CD34^+$ cells	−11±5.2

The cells were infected with Ad35L at 10 000 VP/cell. After incubation for 24 h, CD46 expression on the cell surface was determined by flow cytometry as described in Materials and methods. Values represent mean±s.d. of quadruplicate results from two similar experiments.

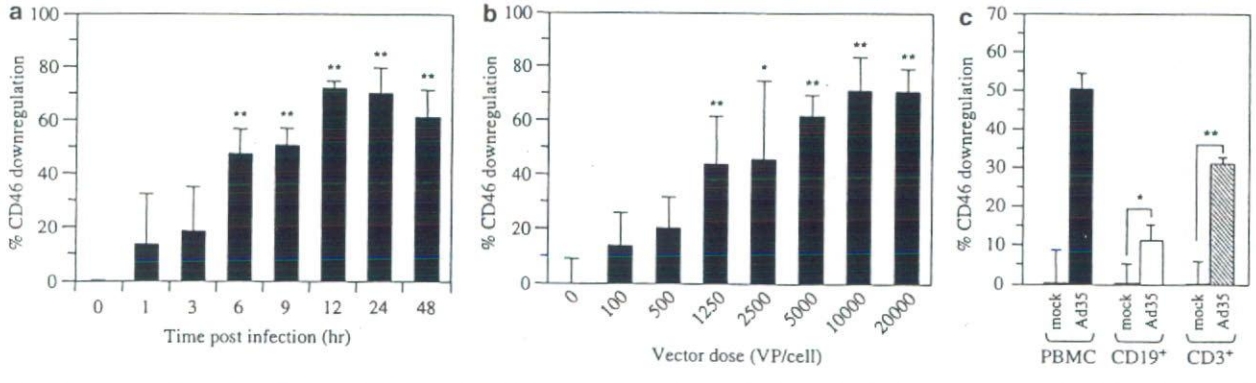

Figure 1 Downregulation of CD46 from the cell surface of PBMCs after infection by Ad35 vectors. (a) Time course of CD46 downregulation from the cell surface of PBMCs after infection with Ad35GFP. PBMCs were incubated with Ad35GFP at 10 000 VP/cell for up to 48 h. Cells were harvested at the indicated time points and stained with anti-human CD46 antibodies after fixation. The expression levels of CD46 on the cell surface were determined by flow cytometry. (b) Dose-dependent downregulation of surface CD46 after infection with Ad35 vectors. PBMCs were infected with Ad35GFP at the indicated vector doses for 24 h. After incubation for 24 h, PBMCs were harvested and CD46 expression levels were determined by flow cytometry. (c) Surface CD46 downregulation in B cells and T cells after infection with Ad35 vectors. PBMCs were infected with Ad35L at 10 000 VP/cell. After incubation for 24 h, PBMCs were harvested and stained with both anti-human CD46 antibody and anti-human CD19 or anti-human CD3 antibody. Subsequently, the cells were subjected to flow cytometric analysis. The asterisks indicate the level of significance ($P<0.005$ (double asterisk), $P<0.05$, (single asterisk)). Values represent mean±s.d. of quadruplicate results from one of at least two similar experiments.

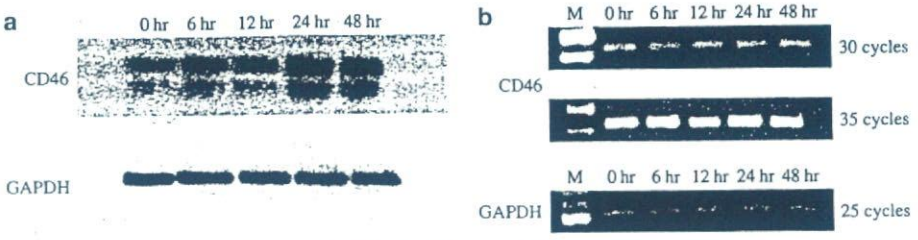

Figure 2 Total cellular protein levels and mRNA levels of CD46 following infection by Ad35 vectors. (a) Western blotting analysis for the total cellular protein levels of CD46 in PBMCs infected with Ad35GFP. PBMCs were incubated with Ad35GFP at 10 000 VP/cell for up to 48 h. Cells collected at the indicated time points were lysed and quantified by immunoblotting for their total cellular amounts of CD46. GAPDH bands served as an internal control for equal total protein loading. This result was representative of three independent experiments. (b) Semiquantitative RT-PCR analysis of CD46 in PBMCs infected with Ad35GFP. PBMCs were infected with Ad35GFP as described for Western blotting analysis in Materials and methods. Total RNA was prepared from PBMCs following incubation with Ad35GFP, and RT-PCR was then performed as described in Materials and methods. Lane M: 100-bp ladder. These results were representative of at least two independent experiments.

and 55% in Molt-4 cells), whereas CD46 expression was reduced not at all or only slightly in nonleukemia cells (A549, HeLa and bone marrow $CD34^+$ cells). Indeed, a slight increase in CD46 expression on the cell surface was found in A549 and $CD34^+$ cells following Ad35 vector infection.

Total protein levels and mRNA levels of CD46 are not reduced following Ad35 vector infection

To examine the mechanism of Ad35 vector-induced downregulation of surface CD46, Western blotting and semiquantitative reverse transcriptase-polymerase chain reaction (RT-PCR) analysis for CD46 expression were performed. Western blotting analysis using total cellular lysates demonstrated that the total cellular levels of CD46 were not reduced, but rather seemed to slightly increase, during 48 h of exposure to Ad35GFP (Figure 2a), suggesting that CD46 may be internalized after infection by Ad35 vectors without intracellular degradation, as in the case of MV.[7] In addition, infection by Ad35GFP did not decrease the mRNA levels of CD46 (Figure 2b). These results indicate that infection by Ad35 vectors does not downregulate the transcription of the *CD46* gene.

Fiber knob proteins of subgroup B Ads play a crucial role in the decrease in surface CD46 expression

To investigate which parts of Ad35 are involved in the downregulation of surface CD46 levels, PBMCs were incubated with conventional Ad5 vectors, fiber-substituted Ad5 vectors displaying the Ad35 fiber shaft and knob, and ultraviolet (UV)- or heat-inactivated Ad35 vectors at 10 000 VP/cell for 24 h. The conventional Ad5 vectors expressing GFP, Ad5GFP, which utilizes CAR for infection, did not downregulate CD46, whereas infection by the Ad5F35 vector expressing GFP, Ad5F35GFP, which recognizes CD46 for infection, significantly reduced surface CD46 expression by 72% (Figure 3a). UV-inactivated Ad35GFP also induced the downregulation of surface CD46 by 62% following infection, which was a level similar to that of surface CD46 downregulation induced by Ad35GFP. However, heat-inactivated Ad35GFP produced a lower level of surface CD46 downregulation than UV-inactivated Ad35GFP. This low level of CD46 downregulation by heat-inactivated Ad35GFP

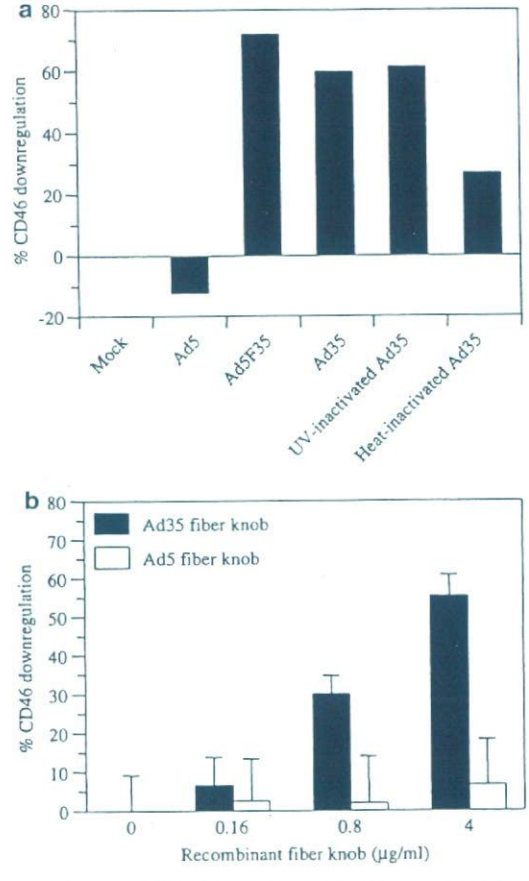

Figure 3 Role of Ad35 fiber knob protein on downregulation of surface CD46. (a) Downregulation of surface CD46 expression induced by various types of Ad vectors. PBMCs were incubated with Ad5GFP, Ad5F35GFP, Ad35GFP, UV-inactivated Ad35GFP or heat-inactivated Ad35GFP at 10 000 VP/cell for 24 h. After incubation, the cells were subjected to flow cytometric analysis to determine the level of CD46 expression. Values represent the mean of duplicate results from one of three similar experiments. (b) Downregulation of surface CD46 expression induced by Ad35 fiber knob protein. PBMCs were incubated with Ad5 or Ad35 fiber proteins at the indicated concentrations. After incubation for 24 h, the cells were subjected to flow cytometric analysis for the measurement of surface CD46 levels. Values represent the mean of quadruplicate results from one of three similar experiments.

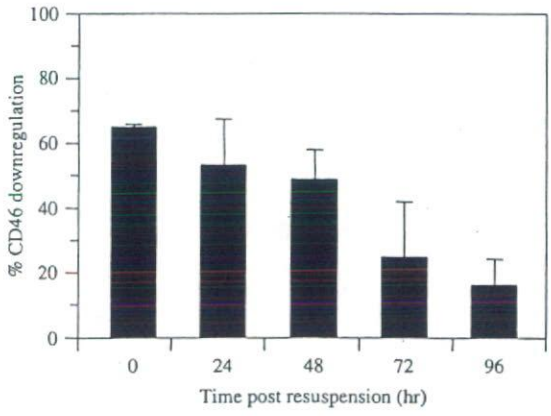

Figure 4 Recovery of surface CD46 expression after Ad35 vector-mediated downregulation. PBMCs were infected with Ad35GFP at 10 000 VP/cell for 24 h. After a 24-h infection, PBMCs were washed twice to remove the Ad35GFP, and resuspended and incubated in fresh medium. After incubation, cells were harvested at the indicated time points and CD46 expression was measured by flow cytometry. Values represent mean ± s.d. of quadruplicate results from one of two similar experiments.

would be due to the thermal denaturation of fiber proteins in Ad35GFP.

Next, PBMCs were incubated with recombinant Ad5 or Ad35 fiber knob proteins to further examine the role of Ad35 fiber protein in the downregulation of surface CD46 expression. Ad35 fiber knob proteins were found to downregulate the surface expression levels of CD46 in a dose-dependent manner, and maximal downregulation of surface CD46 was induced by 55% at 4 μg/ml (Figure 3b). In contrast, no significant reduction in surface CD46 levels was found after incubation with Ad5 fiber knob proteins. These results indicate that fiber knob proteins of Ad35 play a crucial role in the downregulation of surface levels of CD46.

Downregulated CD46 expression is not rapidly restored after the removal of Ad35 vectors

Next, we examined how long it takes to restore surface CD46 expression after Ad35 vector-induced downregulation. Downregulation of surface CD46 induced by Ad35GFP gradually recovered after resuspension, however, the recovery kinetics of CD46 expression after the removal of Ad35 vectors was much lower than the kinetics of Ad35 vector-induced decrease in the surface CD46 (Figure 4). CD46 expression was downregulated by 65% before resuspension, and surface CD46 expression remained reduced by 53 and 49% at 24 and 48 h after resuspension, respectively. Complete restoration of surface CD46 expression was not observed even at 96 h after resuspension, at which point 17% downregulation remained, thus, more than 96 h are required to restore completely surface CD46 expression after Ad35 vector-induced downregulation.

Discussion

Understanding the interaction between cellular receptors and viruses and subsequent events following the attachment of viruses to receptors is important to elucidate the tropism, infectivity and pathogenicity of viruses. Many previous studies have assessed the interaction between CD46 and CD46-utilizing pathogens, especially MV, and have demonstrated that infection by CD46-utilizing pathogens causes unique cellular events. For example, downregulation of CD46 from the cell surface occurs following infection by MV,[7,17] HHV6[4] or *Neisseria*.[9] Additionally, MV and HHV6 suppress interleukin (IL)-12 production in infected human monocytes.[29,30] However, subsequent cellular events following the interaction between human CD46 and subgroup B Ads have not yet been fully evaluated. In the present study, we have demonstrated the downregulation of human CD46 from the cell surface following infection by Ad35 vectors belonging to subgroup B.

MV-induced downregulation of surface CD46 has been the most thoroughly studied aspect of the effects of pathogens recognizing CD46. Nevertheless, the precise mechanisms of MV-induced downregulation of surface CD46 remain to be clarified; surface CD46 downregulation by MV exhibits similar properties to that induced by Ad35 vectors. First, surface expression levels of CD46 are reduced, whereas the total cellular protein levels of CD46 are not significantly decreased after infection,[7] as demonstrated by Western blotting analysis (Figure 2a). These results suggest that CD46 may be internalized without degradation following infection by MV or Ad35. Second, the protein components, which bind to CD46 in the virion, MVH proteins and fiber knob proteins of Ad35, are involved with surface CD46 downregulation. Previous studies indicate that direct protein–protein contact between CD46 and MVH proteins is necessary for the MV-induced downregulation of surface CD46 levels.[31,32] The present data in Figure 3 indicate that fiber knob proteins of Ad35 play a crucial role in the reduction in surface CD46 expression. These common properties suggest that Ad35 might downregulate the surface expression levels of CD46 through a mechanism similar to the one that acts in the case of MV. This hypothesis is further supported by previous findings that both the MVH and fiber knob proteins of Ad35 recognize the domains within SCR1 and 2 of CD46.[13–15,33,34]

However, the Ad35 vector-mediated modulation of CD46 expression in nonleukemia cells differed from that induced by MVH protein: Ad35 vectors did not produce any decline in CD46 expression in the nonleukemia cells used in the present study (HeLa, A549 and human bone marrow-derived $CD34^+$ cells). We have also demonstrated that surface CD46 expression was not decreased following Ad35 vector infection in Chinese hamster ovary (CHO) transformants expressing CD46[15] (data not shown), however, the MVH protein downregulated CD46 expression in HeLa cells[31] and in CHO transformants stably expressing CD46.[35] These findings suggest that cellular events following the binding of Ad35 vectors to CD46 would be somewhat different from those induced by MV in nonleukemia cells.

Downregulation of surface CD46 levels by Ad35 vectors seems inefficient compared with that induced by MV. An approximately 24% reduction in CD46 expression was achieved in U937 cells 24 h following infection of Ad35L at 10 000 VP/cell, which is an approximate multiplicity of infection (MOI) of 50. In contrast, infection by MV strain Edmonston in U937 cells

induced a decline of about 70% in CD46 expression 12 h after infection even at an MOI of 5.[31] The lower levels of surface CD46 downregulation caused by replication-incompetent Ad35 vectors might be partly due to a lack of virus replication; a previous study suggests that newly synthesized MVH proteins in the infected cells further downregulate surface CD46 expression.[31]

Piliated *N. gonorrhoeae*, which also utilizes CD46 as a receptor, exhibits surface CD46 downregulation by the shedding of CD46.[9] The total levels of CD46 in the whole-cell lysates are reduced, and soluble CD46 is found in cell culture supernatants after exposure to piliated *N. gonorrhoeae*. It now remains unclear how piliated *N. gonorrhoeae* induces shedding of CD46. However, it is unlikely that Ad35 vector-induced shedding of CD46 occurs because total cellular levels of CD46 were not reduced following infection with Ad35 vectors (Figure 2a).

It is surprising that the downregulation of surface CD46 expression was not readily restored after the removal of Ad35 vectors because pulse-chase analysis of CD46 showed that matured forms of CD46 are synthesized within 1 h.[36] This raises the question of why newly synthesized CD46 is not transported to the surface membrane in Ad35 vector-infected cells and where newly synthesized CD46 stays in the cells. Further studies are necessary to address these questions.

Previous studies have demonstrated the increased susceptibility of cells to complement-mediated lysis as a result of surface CD46 downregulation,[10,31] however, we found no apparent lysis of PBMCs *in vitro* by complements following Ad35 vector infection (data not shown). It is now unclear why the complement-mediated cell lysis did not occur in cells showing CD46 downregulation by Ad35 vectors. One possible explanation is that the decreased levels of surface CD46 by Ad35 vectors might be enough to block the complement-mediated cell lysis. Other complement regulatory proteins might compensate the reduction in surface CD46 levels. Although PBMCs showing the reduction in surface CD46 density did not exhibit an apparent increase in susceptibility to complement-mediated cell lysis *in vitro*, this study suggests that we should exercise caution in the use of CD46-utilizing Ad vectors. The reduction in CD46 expression in cells transduced with CD46-utilizing Ad vectors might cause unexpected side effects after *in vivo* application. Recently, CD46 has been demonstrated to be involved in not only complement regulation but also various cellular functions, such as immune responses.[37,38] It is essential to further examine the influence of surface CD46 downregulation, including the fate of the transduced cells, before initiating clinical applications of CD46-utilizing Ad vectors. Additionally, the influence of surface CD46 downregulation *in vivo* should be evaluated in nonhuman primates; the use of human CD46-transgenic mice is not recommended because rodent CD46 expression is limited in testis, and other complement regulators, such as decay-accelerating factor, protect cells from complement attack in rodents.[39]

In summary, we have shown that infection by Ad35 vectors induces downregulation of human CD46 from the cell surface in a dose-dependent and cell type-specific manner. In addition to Ad35 vectors, fiber-substituted Ad5 vectors containing fiber proteins derived from Ad35 also downregulate the surface expression of CD46. Once the surface expression levels of CD46 have declined, CD46 expression is not readily restored after the removal of Ad35 vectors. The present study provides important clues for clarifying the pathogenicity of subgroup B Ad, and suggests caution in the use of Ad vectors recognizing CD46 for gene therapy.

Materials and methods

Cells

Human PBMCs (Cambrex Bio Science, Walkersville, MD, USA) were cultured in culture medium (Roswell Park Memorial Institute (RPMI)1640 supplemented with 10 mM *N*-2-hydroxyethylpiperazine-*N'*-2-ethanesulfonic acid, 1 mM sodium pyruvate, 0.1 mM nonessential amino acids, 4 mM L-glutamine, 10% fetal bovine serum (FBS)). HeLa cells (human cervix epitheloid carcinoma) were cultured with Dulbecco's modified Eagle's medium supplemented with 10% FBS. A549 cells (a human lung epithelial cell line) were cultured with F-12K medium supplemented with 10% FBS. K562 cells (human chronic myelogenous leukemia in blast crisis), U937 cells (a human lymphoma cell line), Molt-4 (a human T-cell leukemia cell line) and KG-1a cells (human bone marrow acute myelogenous leukemia) were cultured with RPMI1640 medium supplemented with 10% FBS. Human bone marrow-derived $CD34^+$ cells (Cambrex Bio Science) were cultured with StemSpan 2000 containing cytokine cocktail StemSpan CC100 (human Flt-3 ligand (100 ng/ml), human stem cell factor (100 ng/ml), human IL-3 (20 ng/ml) and human IL-6 (20 ng/ml)) (StemCell Technologies Inc., Vancouver, BC, Canada).

Ad vectors

Ad35 vectors containing a cytomegalovirus promoter-driven enhanced GFP expression cassette or a cytomegalovirus promoter-driven firefly luciferase expression cassette, Ad35GFP and Ad35L, respectively, were constructed by the improved *in vitro* ligation method described previously.[40] GFP-expressing conventional Ad5-based vectors, Ad5GFP and fiber-substituted Ad5-based vectors displaying the fiber knob and shaft of Ad35, Ad5F35GFP, were also constructed as described previously.[25,41] Determination of the virus particle titers of Ad vectors was accomplished following the method described by Maizel *et al*.[42] Ad35GFP was UV- and heat-inactivated by exposure to 254-nm radiation for 1 h, and by incubation at 48°C for 1 h, respectively. The efficiency of the inactivation was confirmed by comparing the transduction efficiencies of control and inactivated Ad35GFP.

Downregulation of surface CD46 by infection with Ad35 vectors

For the present time course study of the downregulation of surface CD46, PBMCs were seeded in a 96-well plate at 5.0×10^4 cells/well and incubated with Ad35GFP at 10 000 VP/cell. PBMCs were harvested at various time points and subjected to flow cytometric analyses as described below. For the study of the dose-dependent downregulation of surface CD46, PBMCs were infected with Ad35GFP at the indicated vector doses. After incubation for 24 h, the surface expression levels of CD46

were measured by flow cytometry. Analysis of the downregulation of surface CD46 levels in response to various types of Ad vectors was similarly performed. Ad35 vector-mediated decrease in the surface CD46 levels was also assessed in various types of human cells (Molt-4, KG-1a, K562, U937, A549, HeLa and human bone marrow-derived CD34$^+$ cells). Cells were seeded in a 24- or 96-well plate and infected with Ad35L at 10 000 VP/cell. After incubation for 24 h, CD46 expression levels were assessed by flow cytometry.

Ad35 fiber knob-mediated downregulation of surface CD46

Recombinant Ad35 fiber knob protein was constructed similarly to Ad5 fiber knob,[43] using Ad35 vector plasmid pAdMS4[44] and the following primers: forward, 5′-tcg aat tca cct tat gga ctg gaa taa acc c-3′ (*Eco*RI site is underlined); reverse, 5′-atg cgg ccg ctt agt tgt cgt ctt ctg taa tgt aag a-3′ (*Not*I site is underlined). Ad5 fiber knob protein was prepared previously.[43] PBMCs, which were seeded in a 96-well plate at 5.0×10^4 cells/well, were incubated with the Ad5 or Ad35 fiber knob at the indicated concentrations. Surface CD46 expression levels were examined 24 h after incubation by flow cytometry as described below.

Western blotting analysis for CD46 expression

PBMCs (5.0×10^5 cells) were seeded in a 24-well plate and infected with Ad35GFP at 10 000 VP/cell. They were then collected at the indicated time points, washed and treated with lysis buffer (25 mM Tris, 1% Triton X-100, 0.5% sodium deoxycholate, 5 mM ethylenediaminetetraacetic acid, 150 mM NaCl) containing a cocktail of protease inhibitors (Sigma, St Louis, MO, USA). The protein content in the cell lysates was measured with an assay kit from Bio-Rad (Hercules, CA, USA), using bovine serum albumin (BSA) as a standard. Protein samples (10 μg) were subjected to nonreducing sodium dodecyl sulfate-12.5% polyacrylamide gel electrophoresis, and the separated proteins were transferred to a nitrocellulose membrane. After blocking nonspecific binding, CD46 was detected with anti-CD46 rabbit serum (1:5000; kindly provided by Dr Tsukasa Seya, Hokkaido University, Japan), followed by incubation in the presence of horseradish peroxidase-labeled goat anti-rabbit second antibody (1:6000, Cell Signaling, Danvers, MA, USA). Signals on the membrane were visualized and analyzed as described previously.[40] To verify equal loading, the blots were stripped and probed with a rabbit anti-glyceraldehyde-3-phosphate dehydrogenase (GAPDH) (1:3000, Trevigen, Gaithersburg, MD, USA) followed by treatment with an horseradish peroxidase-conjugated goat anti-rabbit second antibody (1:5000, Cell Signaling).

RT-PCR analysis for CD46 expression

PBMCs were infected with Ad35GFP as performed in Western blotting analysis. After infection, the cells were collected at the indicated time points and total RNA was isolated from the cells using Isogen reagent (Nippon Gene, Tokyo, Japan). First-strand cDNA templates were synthesized as previously described,[43] and the templates were subjected to PCR amplification using sets of primers for human CD46[45] and GAPDH.[46] The cycling parameters were 30 s at 94°C, 30 s at 55°C and 30 s at 72°C for both CD46 and GAPDH. PCR products were separated by electrophoresis on a 2.0% agarose gel and visualized with ethidium bromide.

Recovery of CD46 expression from the Ad35 vector-mediated downregulation of surface CD46 expression

PBMCs seeded in a six-well plate were infected with Ad35GFP at 10 000 VP/cell. After a 24-h incubation, the cells were collected and washed twice to remove the Ad35GFP. The PBMCs were then resuspended in fresh culture medium, and subsequently cultured at 37°C PBMCs were harvested at the indicated time points and subjected to flow cytometric analysis to measure CD46 expression.

Flow cytometry

Cells were harvested, washed with FACS buffer (phosphate-buffered saline (PBS) containing 1% BSA and 0.01% sodium azide) and then fixed for 10 min with 3.2% paraformaldehyde-containing PBS. Cells were washed twice and incubated with anti-human CD46 antibody (J4.48, Immunotech, Marseilles, France; or E4.3, Pharmigen, San Diego, CA, USA) for 45 min on ice. Subsequently, the cells were washed and incubated with phycoerythrin (PE)-conjugated goat anti-mouse IgG second antibody (Pharmingen). After being washed thoroughly, stained cells were analyzed by FACSCalibur (Becton Dickinson, Tokyo, Japan) and CellQuest software (Becton Dickinson) to obtain the percentage of surface CD46 downregulation as follows: CD46 downregulation = 100−(100 × MFI of CD46 in infected cells)/(MFI of CD46 in uninfected cells), where MFI = mean fluorescence intensity.

For the simultaneous analysis of expression levels of CD46 and CD19 (B-cell marker) or CD3 (T cell marker), PBMCs were incubated with both fluorescein isothiocyanate (FITC)-labeled anti-human CD46 antibody (E4.3, Pharmingen) and PE-conjugated anti-human CD19 antibody (HIB19, Pharmingen) or allophycocyanin (APC)-labeled anti-human CD3 antibody (UCHT1, eBioscience, San Diego, CA, USA). After incubation for 45 min on ice, stained cells were subjected to flow cytometry analysis as described above.

Abbreviations

Ad, adenovirus; APC, allophycocyanin; BSA, bovine serum albumin; CAR, coxsackievirus and adenovirus receptor; FBS, fetal bovine serum; FITC, fluorescein isothiocyanate; GAPDH, glyceraldehyde-3-phosphate dehydrogenase; GFP, green fluorescence protein; HHV6, herpesvirus type 6; MV, measles virus; MVH, measles virus hemagglutinin; MFI, mean fluorescence intensity; MOI, multiplicity of infection; PBMCs, peripheral blood mononuclear cells; PBS, phosphate-buffered saline; RT-PCR, reverse transcriptase-polymerase chain reaction; SCRs, short consensus repeats; VP, vector particle; PE, phycoerythrin.

Acknowledgements

We thank Ms Naoko Funakoshi, Ms Tomomi Sasaki and Ms Noriko Tada for their technical assistance. We also

thank Dr Tsukasa Seya (Hokkaido University, Japan) for providing anti-CD46 rabbit serum. This work was supported by grants for Health and Labour Sciences Research from the Ministry of Health, Labour, and Welfare of Japan, and by Grants-in-Aid for Scientific Research on Priority Areas (B).

References

1 Liszewski MK, Post TW, Atkinson JP. Membrane cofactor protein (MCP or CD46): newest member of the regulators of complement activation gene cluster. *Annu Rev Immunol* 1991; **9**: 431–455.

2 Seya T, Atkinson JP. Functional properties of membrane cofactor protein of complement. *Biochem J* 1989; **264**: 581–588.

3 Dorig RE, Marcil A, Chopra A, Richardson CD. The human CD46 molecule is a receptor for measles virus (Edmonston strain). *Cell* 1993; **75**: 295–305.

4 Santoro F, Kennedy PE, Locatelli G, Malnati MS, Berger EA, Lusso P. CD46 is a cellular receptor for human herpesvirus 6. *Cell* 1999; **99**: 817–827.

5 Rezcallah MS, Hodges K, Gill DB, Atkinson JP, Wang B, Cleary PP. Engagement of CD46 and alpha5beta1 integrin by group A streptococci is required for efficient invasion of epithelial cells. *Cell Microbiol* 2005; **7**: 645–653.

6 Kallstrom H, Liszewski MK, Atkinson JP, Jonsson AB. Membrane cofactor protein (MCP or CD46) is a cellular pilus receptor for pathogenic Neisseria. *Mol Microbiol* 1997; **25**: 639–647.

7 Naniche D, Wild TF, Rabourdin-Combe C, Gerlier D. Measles virus haemagglutinin induces down-regulation of gp57/67, a molecule involved in virus binding. *J Gen Virol* 1993; **74** (Part 6): 1073–1079.

8 Schneider-Schaulies J, Dunster LM, Kobune F, Rima B, ter Meulen V. Differential downregulation of CD46 by measles virus strains. *J Virol* 1995; **69**: 7257–7259.

9 Gill DB, Koomey M, Cannon JG, Atkinson JP. Down-regulation of CD46 by piliated *Neisseria gonorrhoeae*. *J Exp Med* 2003; **198**: 1313–1322.

10 Schnorr JJ, Dunster LM, Nanan R, Schneider-Schaulies J, Schneider-Schaulies S, ter Meulen V. Measles virus-induced down-regulation of CD46 is associated with enhanced sensitivity to complement-mediated lysis of infected cells. *Eur J Immunol* 1995; **25**: 976–984.

11 Gaggar A, Shayakhmetov DM, Lieber A. CD46 is a cellular receptor for group B adenoviruses. *Nat Med* 2003; **9**: 1408–1412.

12 Segerman A, Atkinson JP, Marttila M, Dennerquist V, Wadell G, Arnberg N. Adenovirus type 11 uses CD46 as a cellular receptor. *J Virol* 2003; **77**: 9183–9191.

13 Fleischli C, Verhaagh S, Havenga M, Sirena D, Schaffner W, Cattaneo R *et al*. The distal short consensus repeats 1 and 2 of the membrane cofactor protein CD46 and their distance from the cell membrane determine productive entry of species B adenovirus serotype 35. *J Virol* 2005; **79**: 10013–10022.

14 Gaggar A, Shayakhmetov DM, Liszewski MK, Atkinson JP, Lieber A. Localization of regions in CD46 that interact with adenovirus. *J Virol* 2005; **79**: 7503–7513.

15 Sakurai F, Murakami S, Kawabata K, Okada N, Yamamoto A, Seya T *et al*. The short consensus repeats 1 and 2, not the cytoplasmic domain, of human CD46 are crucial for infection of subgroup B adenovirus serotype 35. *J Control Release* 2006; **113**: 271–278.

16 Wild TF, Buckland R. Functional aspects of envelope-associated measles virus proteins. *Curr Top Microbiol Immunol* 1995; **191**: 51–64.

17 Schneider-Schaulies J, Schnorr JJ, Brinckmann U, Dunster LM, Baczko K, Liebert UG *et al*. Receptor usage and differential downregulation of CD46 by measles virus wild-type and vaccine strains. *Proc Natl Acad Sci USA* 1995; **92**: 3943–3947.

18 Vogels R, Zuijdgeest D, van Rijnsoever R, Hartkoorn E, Damen I, de Bethune MP *et al*. Replication-deficient human adenovirus type 35 vectors for gene transfer and vaccination: efficient human cell infection and bypass of preexisting adenovirus immunity. *J Virol* 2003; **77**: 8263–8271.

19 Roelvink PW, Lizonova A, Lee JG, Li Y, Bergelson JM, Finberg RW *et al*. The coxsackievirus-adenovirus receptor protein can function as a cellular attachment protein for adenovirus serotypes from subgroups A, C, D, E, and F. *J Virol* 1998; **72**: 7909–7915.

20 Sakurai F, Mizuguchi H, Hayakawa T. Efficient gene transfer into human CD34+ cells by an adenovirus type 35 vector. *Gene Therapy* 2003; **10**: 1041–1048.

21 Seshidhar Reddy P, Ganesh S, Limbach MP, Brann T, Pinkstaff A, Kaloss M *et al*. Development of adenovirus serotype 35 as a gene transfer vector. *Virology* 2003; **311**: 384–393.

22 Abrahamsen K, Kong HL, Mastrangeli A, Brough D, Lizonova A, Crystal RG *et al*. Construction of an adenovirus type 7a E1A-vector. *J Virol* 1997; **71**: 8946–8951.

23 Holterman L, Vogels R, van der Vlugt R, Sieuwerts M, Grimbergen J, Kaspers J *et al*. Novel replication-incompetent vector derived from adenovirus type 11 (Ad11) for vaccination and gene therapy: low seroprevalence and non-cross-reactivity with Ad5. *J Virol* 2004; **78**: 13207–13215.

24 Sirena D, Ruzsics Z, Schaffner W, Greber UF, Hemmi S. The nucleotide sequence and a first generation gene transfer vector of species B human adenovirus serotype 3. *Virology* 2005; **343**: 283–298.

25 Mizuguchi H, Hayakawa T. Adenovirus vectors containing chimeric type 5 and type 35 fiber proteins exhibit altered and expanded tropism and increase the size limit of foreign genes. *Gene* 2002; **285**: 69–77.

26 Shayakhmetov DM, Papayannopoulou T, Stamatoyannopoulos G, Lieber A. Efficient gene transfer into human CD34(+) cells by a retargeted adenovirus vector. *J Virol* 2000; **74**: 2567–2583.

27 Krasnykh VN, Mikheeva GV, Douglas JT, Curiel DT. Generation of recombinant adenovirus vectors with modified fibers for altering viral tropism. *J Virol* 1996; **70**: 6839–6846.

28 Stecher H, Shayakhmetov DM, Stamatoyannopoulos G, Lieber A. A capsid-modified adenovirus vector devoid of all viral genes: assessment of transduction and toxicity in human hematopoietic cells. *Mol Ther* 2001; **4**: 36–44.

29 Karp CL, Wysocka M, Wahl LM, Ahearn JM, Cuomo PJ, Sherry B *et al*. Mechanism of suppression of cell-mediated immunity by measles virus. *Science* 1996; **273**: 228–231.

30 Smith A, Santoro F, Di Lullo G, Dagna L, Verani A, Lusso P. Selective suppression of IL-12 production by human herpesvirus 6. *Blood* 2003; **102**: 2877–2884.

31 Schneider-Schaulies J, Schnorr JJ, Schlender J, Dunster LM, Schneider-Schaulies S, ter Meulen V. Receptor (CD46) modulation and complement-mediated lysis of uninfected cells after contact with measles virus-infected cells. *J Virol* 1996; **70**: 255–263.

32 Lecouturier V, Rizzitelli A, Fayolle J, Daviet L, Wild FT, Buckland R. Interaction of measles virus (Halle strain) with CD46: evidence that a common binding site on CD46 facilitates both CD46 downregulation and MV infection. *Biochem Biophys Res Commun* 1999; **264**: 268–275.

33 Iwata K, Seya T, Yanagi Y, Pesando JM, Johnson PM, Okabe M *et al*. Diversity of sites for measles virus binding and for inactivation of complement C3b and C4b on membrane cofactor protein CD46. *J Biol Chem* 1995; **270**: 15148–15152.

34 Manchester M, Valsamakis A, Kaufman R, Liszewski MK, Alvarez J, Atkinson JP *et al*. Measles virus and C3 binding sites are distinct on membrane cofactor protein (CD46). *Proc Natl Acad Sci USA* 1995; **92**: 2303–2307.

35 Bartz R, Firsching R, Rima B, ter Meulen V, Schneider-Schaulies J. Differential receptor usage by measles virus strains. *J Gen Virol* 1998; **79** (Part 5): 1015–1025.

36 Liszewski MK, Tedja I, Atkinson JP. Membrane cofactor protein (CD46) of complement. Processing differences related to alternatively spliced cytoplasmic domains. *J Biol Chem* 1994; **269**: 10776–10779.

37 Oliaro J, Pasam A, Waterhouse NJ, Browne KA, Ludford-Menting MJ, Trapani JA *et al*. Ligation of the cell surface receptor, CD46, alters T cell polarity and response to antigen presentation. *Proc Natl Acad Sci USA* 2006; **103**: 18685–18690.

38 Kemper C, Verbsky JW, Price JD, Atkinson JP. T-cell stimulation and regulation: with complements from CD46. *Immunol Res* 2005; **32**: 31–43.

39 Harris CL, Spiller OB, Morgan BP. Human and rodent decay-accelerating factors (CD55) are not species restricted in their complement-inhibiting activities. *Immunology* 2000; **100**: 462–470.

40 Sakurai F, Kawabata K, Koizumi N, Yamaguchi T, Hayakawa T, Mizuguchi H. Adenovirus serotype 35 vector-mediated transduction into human CD46-transgenic mice. *Gene Therapy* 2006; **13**: 1118–1126.

41 Mizuguchi H, Koizumi N, Hosono T, Utoguchi N, Watanabe Y, Kay MA *et al*. A simplified system for constructing recombinant adenoviral vectors containing heterologous peptides in the HI loop of their fiber knob. *Gene Therapy* 2001; **8**: 730–735.

42 Maizel Jr JV, White DO, Scharff MD. The polypeptides of adenovirus. I. Evidence for multiple protein components in the virion and a comparison of types 2, 7A, and 12. *Virology* 1968; **36**: 115–125.

43 Koizumi N, Mizuguchi H, Hosono T, Ishii-Watabe A, Uchida E, Utoguchi N *et al*. Efficient gene transfer by fiber-mutant adenoviral vectors containing RGD peptide. *Biochim Biophys Acta* 2001; **1568**: 13–20.

44 Sakurai F, Kawabata K, Yamaguchi T, Hayakawa T, Mizuguchi H. Optimization of adenovirus serotype 35 vectors for efficient transduction in human hematopoietic progenitors: comparison of promoter activities. *Gene Therapy* 2005; **12**: 1424–1433.

45 Rushmere NK, Knowlden JM, Gee JM, Harper ME, Robertson JF, Morgan BP *et al*. Analysis of the level of mRNA expression of the membrane regulators of complement, CD59, CD55 and CD46, in breast cancer. *Int J Cancer* 2004; **108**: 930–936.

46 Dash S, Saxena R, Myung J, Rege T, Tsuji H, Gaglio P *et al*. HCV RNA levels in hepatocellular carcinomas and adjacent non-tumorous livers. *J Virol Methods* 2000; **90**: 15–23.

J Pharmacol Sci 103, 159 – 167 (2007)

Journal of Pharmacological Sciences

Full Paper

Caspase Cascade Proceeds Rapidly After Cytochrome *c* Release From Mitochondria in Tumor Necrosis Factor-α-Induced Cell Death

Hiroshi Kawai[1,3,*], Takuo Suzuki[1], Tetsu Kobayashi[1], Akiko Ishii-Watabe[1], Haruna Sakurai[2], Hisayuki Ohata[2], Kazuo Honda[2], Kazutaka Momose[2], Takao Hayakawa[1], and Toru Kawanishi[1,#]

[1]*Division of Biological Chemistry and Biologicals, National Institute of Health Sciences, Tokyo 158-8501, Japan*
[2]*Department of Pharmacology, School of Pharmaceutical Sciences, Showa University, Tokyo 142-8555, Japan*
[3]*Faculty of Pharmaceutical Sciences, Josai International University, Chiba 283-8555, Japan*

Received August 2, 2006; Accepted December 2, 2006

Abstract. The caspase activation cascade and mitochondrial changes are major biochemical reactions in the apoptotic cell death machinery. We attempted to clarify the temporal relationship between caspase activation, cytochrome *c* release, mitochondrial depolarization, and morphological changes that take place during tumor necrosis factor (TNF)-α-induced cell death in HeLa cells. These reactions were analyzed at the single-cell level with 0.5 – 1 min resolution by using green fluorescent protein (GFP)-variant-derived probes and chemical probes. Cytochrome *c* release, caspase activation, and cellular shrinkage were always observed in this order within 10 min in all dying cells. This sequence of events was thus considered a critical pathway of cell death. Mitochondrial depolarization was also observed in all dying cells observed, but frequently occurred after caspase activation and cellular shrinkage. Mitochondrial depolarization is therefore likely to be a reaction that does not induce caspase activation and subsequent cellular shrinkage. Mitochondrial changes are important for apoptotic cell death; moreover, cytochrome *c* release, and not depolarization, is a key reaction related to cell death. In addition, we also found that the apoptotic pathway proceeds only when cells are exposed to TNF-α. These findings suggest that the entire cell death process proceeds rapidly during TNF-α exposure.

Keywords: tumor necrosis factor (TNF)-α, cytochrome *c*, mitochondrial depolarization, caspase, real-time imaging

Introduction

Apoptosis is a mechanism of cell death that is mediated by various intracellular reactions. A family of cysteine proteases, the caspases, forms the activation cascade, and these proteases play a central role in the apoptotic cell death machinery (1, 2). The caspases usually exist as pro-proteins in living cells and are activated by cleavage at the time when cell death is induced. In an early phase of the cell death process, initiator caspases are activated, which in turn activate effector caspases (3 – 7). Activated effector caspases cleave a number of different target proteins, and this cleavage leads ultimately to apoptotic cell death (8, 9). Mitochondria also play an important role in the cell death process (10 – 13). Cellular stresses induce mitochondrial changes, including an increase in outer mitochondrial membrane permeability; various mitochondrial proteins such as cytochrome *c* (cyt.*c*) and second mitochondrial activator of caspases (Smac) are released into the cytosol. Released proteins directly or indirectly regulate caspase activation and/or other reactions, which eventually induce cell death.

Various factors in the cell death process have been identified, but correlation among these factors remains unclear. Cell death events such as caspase activation and mitochondrial changes are rapid processes, and the onset of these events varies between individual cells (14 – 17). So, it is difficult to determine how and when such

*Corresponding author (affiliation #3). hkawai@jiu.ac.jp
#Present affiliation: Division of Drugs, National Institute of Health Sciences, Tokyo 158-8501, Japan
Published online in J-STAGE: February 8, 2007
doi: 10.1254/jphs.FP0060877

reactions occur in cells as based on analyses of cell populations, which can only be used to detect an average value for a large number of individual cells. In order to gain a better understanding of the cell death mechanism, simultaneous multi-events analyses should be conducted at the single-cell level and with high spatial and temporal resolution. Real-time imaging with confocal microscopy is a powerful method of detecting the manner in which such rapid intracellular reactions take place (18, 19).

Fluorescence resonance energy transfer (FRET) is useful for imaging analyses. Variants of green fluorescent protein (GFP) are currently widely employed; several families of fluorescent proteins have recently been reported to be useful for FRET analysis (19 – 22). Previously, we developed genetically-encoded sensors for caspase activation that consist of two fluorescent proteins linked by a small peptide (23, 24). Cyan-, green-, yellow-, and red-fluorescent proteins (CFP, GFP, YFP, DsRed) were used in combination as the fluorescent proteins. The small peptide was derived from a substrate of caspase, poly(ADP-ribose)polymerase; this fusion protein was primarily cleaved by caspase 3 (23). The sensor protein exhibits FRET in its intact form. However, in the presence of active caspase, the peptide is cleaved, and the two fluorescent proteins are rendered far apart; in this case, the sensor protein no longer exhibits any FRET. Caspase activation is detected as a reduction in FRET. We have previously reported that the use of various color combinations facilitates real-time imaging analysis. In particular, GFP-DsRed and YFP-DsRed have been shown to be as sensitive as CFP-YFP, which is commonly used as the FRET pair. FRET probes that consist of such color variations may be useful for simultaneous multi-event imaging (24).

In this study, we used the YFP-DsRed version of the effector-caspase sensor (YRec), CFP-tagged cyt.*c* (cyt.*c*-CFP), and tetramethylrhodamine methyl ester (TMRM) in order to detect caspase activation, cyt.*c* release from the mitochondria, and mitochondrial depolarization, respectively. By applying two of these probes simultaneously, two events could be monitored in the same cell, and the temporal relationships between caspase activation and mitochondrial changes could be examined at the single-cell level. In addition, we also analyzed the interval from tumor necrosis factor (TNF)-α exposure to cellular shrinkage by analyzing the cell population in order to investigate time course of the whole cell death process.

Materials and Methods

Plasmid construction

A plasmid encoding YRec, YFP-peptide-DsRed, was generated as previously reported (24). The sequence encoding the 11 amino acids at the C-terminus of YFP was eliminated in this construct. The C-terminal-truncated forms of the YFP gene were generated by PCR with primers containing the NheI site or the BspEI site and pEYFP-C1 (Clontech, Palo Alto, CA, USA) as a template, and the restricted fragment was inserted into the NheI/BspEI sites of pEYFP-C1 in order to generate a plasmid carrying truncated YFP. The oligonucleotides encoding the caspase's substrate sequence was inserted into the BspEI – AgeI site of the p(truncated YFP)-C1 vector to generate pYFP-PARP. The substrate sequence was derived from PARP (KRKGDEVDGVDE, 5'-CCGGAAAGAGAAAAGG CGATGAGGTGGATGGAGTGGATGAA-3' and 5'-CCGGTTCATCCACTCCATCCACCTCATCGCCTTT TCTCTTT-3'). DsRed was generated from pDsRed2-C1(Clontech) by PCR, at the AgeI/NotI sites, and the restricted fragment was inserted into the AgeI – NotI sites of pYFP-PARP to generate a plasmid carrying YFP-PARP-DsRed2 (YRec). YRec was cleaved by caspase-3 (23, 24).

Cyt.*c* was cloned from HeLa cells by RT-PCR with a primer pair (5'-TCGCTAGCGCTCCGGAGAATTAAA TATGGGTATG-3' and 5'-CGAGGATCCCTCATTAG TAGCTTTTTTGAG-3'), and the restricted fragment was inserted into the NheI – BamHI sites of the pECFP-N1 vector to generate a plasmid carrying cyt.*c*-CFP. All cloned sequences were verified by sequencing.

Cell culture and transfection

HeLa cells were cultured in DMEM (Sigma-Aldrich, St. Louis, MO, USA) supplemented with 100 units/ml of penicillin G, 100 μg/ml of streptomycin, and 10% fetal calf serum (GIBCO). The plasmid encoding the fluorescent probes was transfected into HeLa cells using Effectene Transfection Reagent (QIAGEN, Hilden, Germany) according to the manufacturer's instructions. After being incubated for 12 – 24 h with the transfection reagent, the cells were washed with PBS and cultivated on dishes suitable for an assay in medium containing 500 μg/ml of G418 for an additional 1 – 3 days until the assay was performed. We found that the cultivation period had no effect on cell death events after TNF-α treatment.

Bioimaging with fluorescence microscopy

Transfected cells were cultured on a cover glass (25-mm diameter, 0.15 – 0.18-mm thickness) for 1 – 3 days. Cells were treated with TNF-α (100 ng/ml, dissolved in PBS) and cycloheximide (10 μg/ml, dissolved in DMSO) and then were incubated under the usual culture conditions for 1 – 2 h prior to the analysis.

Table 1. Measurement conditions for real-time analysis by LSM510

Probe	Excitation (nm)	Beam splitter (nm)	Emission (nm)
Cyt.*c*-CFP	458	515	467.5 – 497.5
YRec	488	545	505 – 530 (donor)[a]
			560 – 615 (acceptor)[a]
TMRM	543	545	560 –[b]

[a]Emitted fluorescence was separated by a 545 dichroic mirror, and the fluorescence of the donor (YFP) and that of the acceptor (DsRed) was obtained via a band-pass emission filter. [b]A long-pass filter (LP560) was used.

Tetramethylrhodamine methyl ester (TMRM; 50 nM, dissolved in DMSO) was added to each sample 20 – 30 min prior to the analysis, when the mitochondrial membrane potential was to be measured (23, 25). Analyses were carried out by confocal laser scanning fluorescent microscopy using a Carl Zeiss LSM510 system (Carl Zeiss, Jena, Germany). During the observations, the media were buffered with 10 mM HEPES buffer (pH 7.4), and the cells were maintained at 35°C – 37°C. DIC images and grayscale images for fluorescence channels were obtained in 0.5- or 1-min intervals. Excitation lights for the cyt.*c*-CFP (458 nm) and YRec (488 nm) were provided by an Ar laser with a 458 or a 488 dichroic mirror, respectively. Excitation lights for the TMRM (543 nm) were provided by a HeNe laser with a 543 dichroic mirror. Images of the probes were obtained separately using a dichroic mirror and band-pass or long-pass emission filters, as indicated in Table 1. Contamination of the fluorescence between channels was negligible under these conditions (data not shown). For analyses involving YRec or TMRM, images were processed and quantified using MetaFluor software as follows: The average pixel intensity of the fluorescence of the entire cell region was determined for each channel. In the case of YRec, the ratio value was calculated as the average pixel value of the fluorescence ratio, (fluorescent intensity for the acceptor channel) /(fluorescent intensity for the donor channel), in the entire cell region. As the cells changed morphologically during the observation, the entire cell region was assessed separately for each image.

Simultaneous measurement of two probes was performed according to the multi-track scanning mode, in which two sets of excitation-detection conditions were used in alternation. For cyt.*c*-CFP and YRec, CFP fluorescence induced by excitation at 458 nm was measured in the first track, and YFP and DsRed fluorescence induced by excitation at 488 nm was measured in the second track. For cyt.*c*-CFP and TMRM, CFP fluorescence induced by excitation at 458 nm was measured in the first track, and TMRM fluorescence induced by excitation at 543 nm was measured in the second track. The scanning time difference between tracks was ca. 3 – 8 s, which was not significant in the temporal analysis.

Analysis of cell survival rate

HeLa cells were cultured in 96-well plastic plates to 80% – 90% confluency and were then treated with TNF-α. After the indicated culture durations, the cells were treated with Alamar Blue (Dainippon Pharmaceutical, Osaka) according to the manufacturer's instructions. Cell survival was measured as fluorescence at 590 nm induced by excitation at 540 nm. Fluorescence was measured using FlexStation (Molecular Devices, Sunnyvale, CA, USA).

Results

Simultaneous imaging of cyt.c-CFP and caspase sensor

HeLa cells expressing both cyt.*c*-CFP and YRec were treated with TNF-α, and changes in fluorescence were observed. Figure 1A shows DIC images, fluorescent images of CFP, and fluorescence ratio (DsRed/YFP) images of YRec during cell death. Images were obtained every 30 s; therefore, we were able to identify the time points of these events at a resolution period of 30 s. The CFP fluorescence indicated cyt.*c*-CFP localization, and the fluorescence ratio (DsRed/YFP) indicated caspase activation. CFP fluorescence was localized in the mitochondria at 280.5 min, and it was delocalized at 281.0 min, indicating that cyt.*c*-CFP was released during this period. The images shown in Fig. 1A indicate that this cell started to shrink at 286.5 – 287.0 min.

When the caspase was activated in a cell, the YRec was cleaved, which led to a reduction in the FRET from YFP to DsRed. Thus, a reduction in the fluorescence ratio (DsRed/YFP) reflected caspase activation. As shown in Fig. 1B, the fluorescence ratio decreased dramatically at 283.5 min in the cell shown here, thus indicating the initiation of caspase activation at this point in time. The increase in DsRed fluorescence

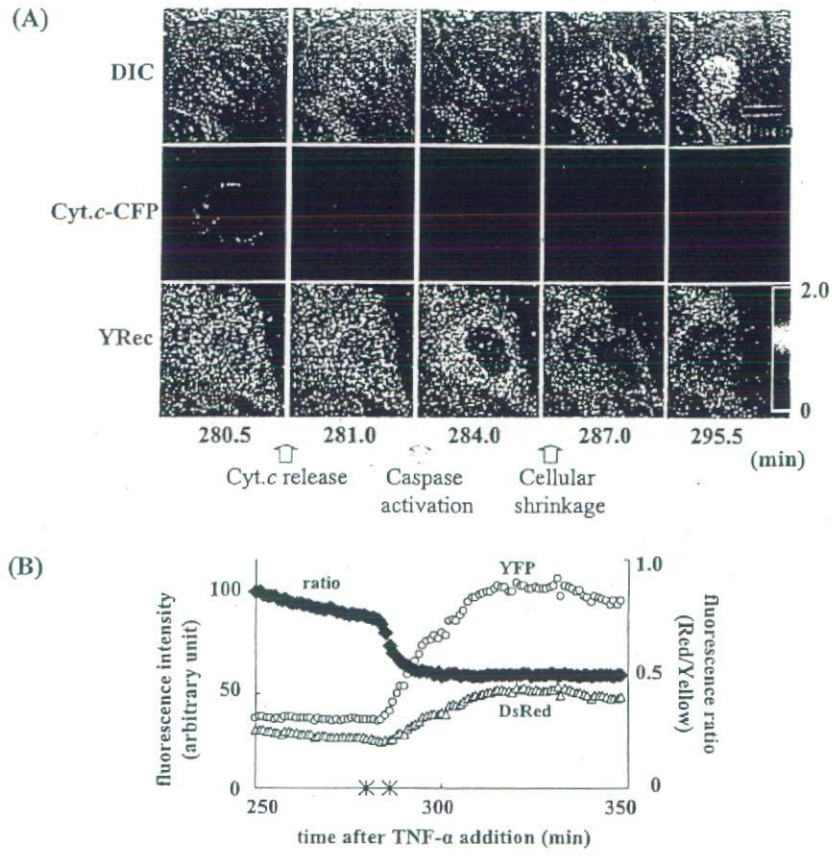

Fig. 1. Cyt.*c*-CFP release and caspase activation were monitored simultaneously in the same cells. A: DIC (upper), images showing the fluorescence of CFP (middle) and the fluorescence ratio of DsRed and YFP (DsRed /YFP, lower) during cell death are shown in pseudocolor. CFP and DsRed/YFP indicate the localization of cyt.*c*-CFP and caspase activation, respectively. B: Changes in YRec fluorescence in the cell shown in panel A were plotted. YFP and DsRed are shown with their fluorescence ratios. The asterisks indicate time points at which cyt.*c*-CFP were released and cell shrinkage was observed. The horizontal axis represents the point in time after the addition of TNF-*α*.

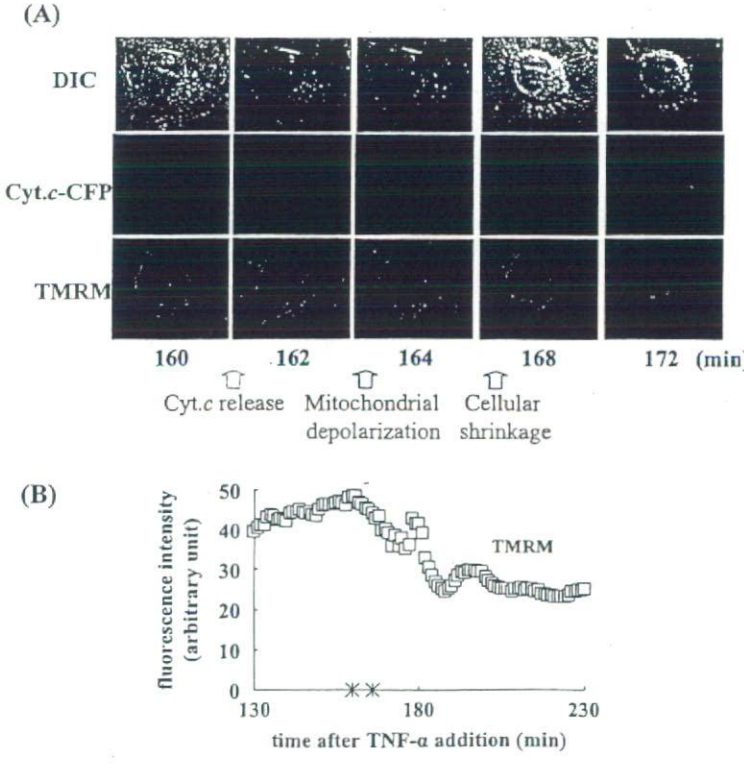

Fig. 2. Cyt.*c*-CFP release and mitochondrial depolarization were monitored simultaneously in the same cell. A: DIC (upper), images showing the fluorescence of CFP (middle) and the fluorescence of TMRM (lower) during cell death are shown in pseudocolor. CFP and TMRM fluorescence indicate the localization of cyt.*c*-CFP and the mitochondrial membrane potential, respectively. B: Changes in TMRM fluorescence of the cells in panel A during cell death were plotted. The asterisks indicate time points at which cyt.*c*-CFP were released and cell shrinkage was observed. The horizontal axis represents the point in time after the addition of TNF-*α*.

observed after this time point was unexpected, but is thought to have been the result of cellular shrinkage. Because the cell volume was reduced, the DsRed became concentrated, and the fluorescence increased. The reduction in the fluorescence ratio clearly indicated a reduction in FRET, which indicated both the cleavage of YRec as well as caspase activation. The asterisks indicate the time point of cyt.*c*-CFP release and cellular shrinkage, as determined based on the results shown in Fig. 1A. In this cell, cyt.*c*-CFP was released 280.5 min after the addition of TNF-α, and caspase activation was initiated 3 min after cyt.*c*-CFP release; the cell then started to shrink 3 min after caspase activation. Cyt.*c*-CFP release, caspase activation, and cellular shrinkage were observed in this order in all of the dying cells examined.

Simultaneous imaging of cyt.c-CFP and TMRM

HeLa cells expressing cyt.*c*-CFP were treated with TMRM and TNF-α. Delocalization of cyt.*c*-CFP and mitochondrial depolarization were observed with a resolution period of 1 min. All dying cells exhibited cyt.*c*-CFP release, mitochondrial depolarization, and shrinkage of the cell body. Figure 2A shows a typical fluorescent image of a dying cell. In this cell, cyt.*c*-CFP was released at 161 min, and cell shrinkage began at 167 min after the addition of TNF-α. Changes in TMRM fluorescence are plotted in Fig. 2B. TMRM fluorescence started to decrease at 164 min, thus indicating that the mitochondria started to depolarize at this point in time.

In a comparison of the starting points of these three events, it was found that the release of cyt.*c*-CFP always preceded mitochondrial depolarization and cellular shrinkage. Mitochondrial depolarization was observed earlier than cellular shrinkage in this particular cell, but was observed later in other cells. The temporal order of the timing of the initiation of mitochondrial depolarization and cellular shrinkage was not consistent. Mitochondrial depolarization preceded cellular shrinkage in 4 of the 10 cells, and cellular shrinkage preceded mitochondrial depolarization in 6 of the cells observed here.

Temporal relationships between mitochondrial changes, caspase activation, and cellular shrinkage

We observed 10 – 22 cells in each of these experiments, the results of which are shown in Figs. 1 and 2. We then determined the timing of cyt.*c* release, cellular shrinkage, and mitochondrial depolarization, or caspase activation in each cell. To clarify the temporal relationships between these cellular events, relative timing was

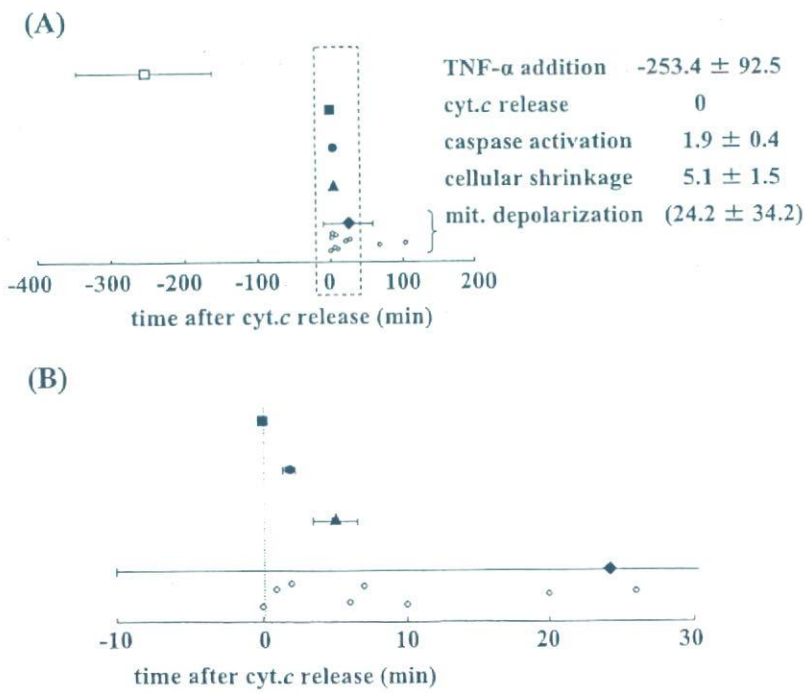

Fig. 3. Temporal relationship between mitochondrial changes and caspase activation. A: Relative timing of TNF-α addition (open square), cyt.*c* release (closed square), caspase activation (closed circle), cellular shrinkage (closed triangle), and mitochondrial depolarization (closed and open diamond) is shown with respect to time after cyt.*c* release. B: Shows a magnification of panel A.

determined as follows: the time point of cyt.*c* release was considered as time 0 in each of the individual cells. We calculated the relative timing of each of the observed events for each cell, and the results are plotted in Fig. 3. TNF-α treatment, cyt.*c* release, caspase activation, and cellular shrinkage are indicated as the mean ± S.D. Since mitochondrial depolarization did not give a normal distribution, all data for mitochondrial depolarization were plotted. Each plot represents the results from a single cell. Figure 3B shows magnification at around time 0.

The relative timing of TNF-α treatment and mitochondrial depolarization was found to deviate substantially, whereas the relative timing of caspase activation and cellular shrinkage gave only a small deviation. A substantial amount of time was required for the initiation of cyt.*c* release, and the duration varied between cells; however, after cyt.*c* release, the subsequent reactions occurred rapidly. After cyt.*c* release, cells are unable to stop or delay the cell death process.

Mitochondrial depolarization occurred before both caspase activation and cellular shrinkage in some of the cells (n = 4), but mitochondrial depolarization occurred after caspase activation and cellular shrinkage in other cells (n = 6). This finding suggests that mitochondrial depolarization is not necessary for either caspase activation or cellular shrinkage. Mitochondrial depolarization has been consistently reported as being associated with cell death, but it is not thought to be a critical step in the induction of apoptotic cell death.

Effects of the duration of TNF-α treatment

At the first step of TNF-α-induced cell death, TNF-α binds with its receptor on the cell surface, and an extracellular signal is transferred into the cell. After this step, Bid transfers the signal to the mitochondria, and then cyt.*c* is released from the mitochondria to the cytosol. Our results shown in Fig. 3 indicate that these processes took about 4 h. In order to analyze the timing of the onset of the earliest steps, we attempted to determine the point in time at which the first step started. To this end, we changed the duration of TNF-α exposure and measured the resulting cell survival rate. Cells were divided to two groups, as shown in Fig. 4A, and the cells were exposed to TNF-α for 0 – 12 h. In group A, the survival rate was measured immediately after TNF-α exposure. In group B, TNF-α was washed off after the indicated exposure time, and the cells were cultured in fresh medium without TNF-α for an additional 6 – 11 h, and the survival rate was then measured. If the cell death process proceeded after the removal of TNF-α, the survival rate would be expected to be reduced due to the additional culture period after the removal of TNF-α. In other words, more cells would be expected to have died in group B than in group A with the same amount of TNF-α exposure time.

The results showed that the survival rate decreased with increasing TNF-α exposure time (Fig. 4B). However, the survival rate did not decrease after TNF-α removal. This result suggests that the dead cells in group B had died during the period of TNF-α exposure, and that those cells that had survived during TNF-α exposure did not die after the removal of TNF-α. Thus, the cell death process is likely to proceed only when the cells were exposed to TNF-α. The survival rate in group B increased when cells were exposed TNF-α for 6 h. The biological meaning of this increase was unknown; however, this result did not disturb our conclusion.

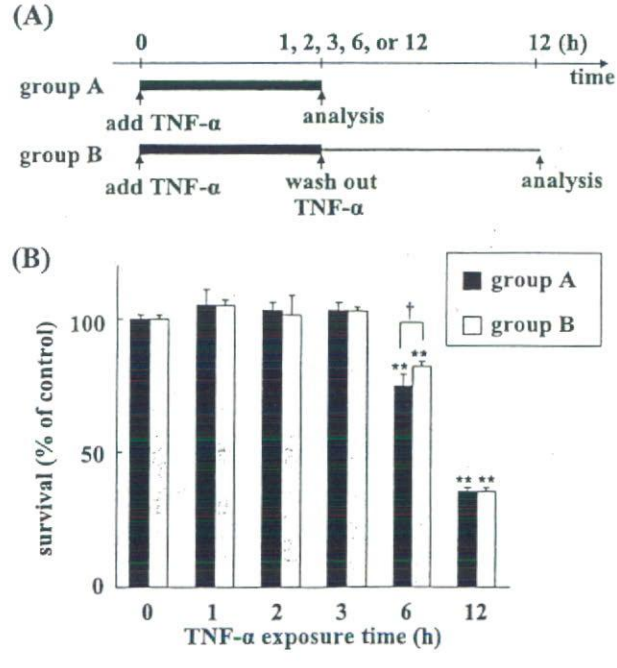

Fig. 4. Cell survival rate after TNF-α exposure. Panel A: Experimental design of the TNF-α exposure analysis. Thick lines represent the incubation in the presence of TNF-α, and thin line represents the incubation in the absence of TNF-α. In group A, cells were exposed to TNF-α for the indicated amount of time, and the cell survival rate was measured immediately. In group B, cells were exposed in the same manner as that used for group A. Then, the TNF-α was washed out, and the cells were cultured in fresh media for 6 – 11 h. Then, the cell survival rate was measured. The total duration of the culture period after the onset of TNF-α exposure was 12 h in group B. Panel B: The cells in groups A and B were exposed to TNF-α for 1, 2, 3, 6, or 12 h, and the cell survival rates were determined. Each bar represents a mean ± S.D. (n = 6). $^{**}P<0.01$ *vs* time 0, according to Dunnett's test. $^{\dagger}P<0.05$ between groups A and B, according to Student's *t*-test.

Discussion

This is the first report to reveal the precise temporal relationships between four reactions (mitochondrial depolarization, cyt.*c* release, caspase activation, and cellular shrinkage) in TNF-α-induced cell death. Because the onset of these reactions varied among individual cells, real-time single-cell imaging is the only currently available method to reveal temporal relationships between these reactions. We described our three-color real-time imaging technique in this report. Rehm et al. has reported the simultaneous real-time imaging of caspase activation and Smac release by using CFP/YFP-FRET sensor and YFP-tagged protein (26). They used the same color, YFP, for the observation of both reactions. It is possible to identify two reactions as they discussed, but it may be difficult to identify small changes occurring in the cell by their method. Previously, we revealed that DsRed was useful for FRET analysis of caspase activation (24). In this report, we observed caspase activation and cyt.*c* release with YFP/DsRed-FRET sensor and CFP-tagged protein. By using fluorescent probes in different colors, each reaction could be easily and precisely identified in a single cell.

We observed cell death at the single-cell level with a resolution period of 0.5 – 1 min, and we revealed that the relative timing between cyt.*c* release, caspase activation, and cellular shrinkage remained constant in all of the dying cells observed; however, the timing of mitochondrial depolarization showed a large deviation (Fig. 3). After cyt.*c* release, apoptosome formation, caspase-9 activation, caspase-3 activation, and the cleavage of various substrates that lead to apoptotic cell death are initiated. Our results revealed that this series of reactions takes place within 10 min and that the time course of this process was identical among all of the dying HeLa cells.

Mitochondrial depolarization was observed in all dying cells, but we considered that mitochondrial depolarization was not the cause of cyt.*c* release, caspase activation, and cellular shrinkage. Mitochondrial depolarization was found to occur at any time after cyt.*c* release. Mitochondrial depolarization was observed after caspase activation and cellular shrinkage in 60% of the observed cells. These results exclude the possibility that mitochondrial depolarization is a cause of cyt.*c* release, caspase activation, and/or cellular shrinkage. This is consistent with previous findings that cell death occurred without mitochondrial depolarization. Li et al. have shown that caspases are activated independently of mitochondrial depolarization in TNF-α-induced cell death (27). Krohn et al. have shown that cyt.*c* release and caspase activation occurred in the absence of mitochondrial depolarization in cell death of hippocampal neurons (28). Several studies suggested that mitochondrial depolarization is a critical step for cell death (29), but our results support the idea that mitochondrial depolarization is not crucial to the cell death process.

Cyt.*c* release may be a key step in two independent series of events, that is, the cell death process and mitochondrial depolarization. We speculate that cells might try to maintain cellular homeostasis by keeping membrane potential after cyt.*c* release. While maintaining the membrane potential, the released cyt.*c* immediately initiated the cell death process in the cytosol, and thus caspase activation and cellular shrinkage always took place within a short period of time. The timing of mitochondrial depolarization did not appear to be relevant to this process.

A number of imaging analyses have demonstrated that each cell death event is a rapid process. Initiator- and effector-caspase activation both proceed rapidly (23, 24, 30 – 32). Cyt.*c* is also released rapidly in a single step (33 – 35). Likewise, Smac/DIABLO is released rapidly, although the duration of Smac/DIABLO release is greater than that of cyt.*c* (26). Several multi-event imaging studies have suggested that cell death events occur almost simultaneously. Initiator caspase activation/effector caspase activation, effector caspase activation/mitochondrial depolarization, cyt.*c*/smac, and effector caspase activation/smac release had been analyzed simultaneously at the single-cell level and were found to occur almost simultaneously (24, 26). These findings, taken together with our present results, suggest that the cell death cascade proceeds rapidly after mitochondrial changes take place.

Once cyt.*c* was released, the following reactions proceed in a rapid manner. However, it did take 253.4 ± 92.5 min from TNF-α treatment to cyt.*c* release, and this duration varied from cell to cell (Figs. 3 and 4). We observed some cells that had died within 1 h in imaging analysis, indicating that cells have the ability to induce cell death within 1 h, and suggesting that certain factors may delay signal transduction and the timing of cell death. The results shown in Fig. 4 indicate that these factors were active only when the cells were exposed to TNF-α. We considered two possible explanations for these findings. 1: Each TNF-α molecule changed the cell slightly, and the changes induced by one molecule were not sufficient to induce the cell death cascade on their own. However, many TNF-α molecules attacked the cell, and intracellular changes thus accumulated. When the accumulated changes exceeded the threshold level, the cell death cascade would be expected to have